THE ASTROPHYSICAL JOURNAL, 463:L71–L74, 1996 June 1

A TWO-DIMENSIONAL SIMULATION OF A RELATIVISTIC MAGNETIZED JET

SHINJI KOIDE
Laboratory of Plasma Astrophysics and Fusion Science, Faculty of Engineering, Toyama University, Gofuku, Toyama 930, Japan
KEN-ICHI NISHIKAWA
Department of Space Physics and Astronomy, Rice University, Houston, TX 77251
AND
ROBERT L. MUTEL
Department of Physics and Astronomy, University of Iowa, Iowa City, IA 52242
Received 1996 January 2; accepted 1996 March 18

ABSTRACT

We have performed a magnetohydrodynamic simulation of a relativistic jet in slab geometry. The simulation code employs a simplified total variation diminishing method. We compare the weakly and strongly magnetized relativistic jets. The result shows that both relativistic effects and the parallel magnetic field collimate the jets. Stronger reversed magnetic fields are formed in the weakly magnetized jet than in the strongly magnetized jet.

Subject headings: galaxies: jets — magnetic fields — MHD — relativity

1. INTRODUCTION

Relativistic jets from active galactic nuclei (AGNs), such as quasars and BL Lacertae objects (Gabuzda, Wardle, & Roberts 1989; Mutel et al. 1990; Cawthorne 1991), have been observed by VLBI. Numerical simulations of jets have been very successful in the study of jet morphology, but most of them have employed nonrelativistic codes (Hardee 1987; Hardee & Clarke 1995; see review by Burns, Norman, & Clarke 1991). VLBI observations and the nonrelativistic simulations have also revealed the importance of magnetic fields in the dynamics of jets. For example, some bending jets, such as 3C 279 and 3C 454.3, and almost all BL Lacertae objects, are explained by the interaction between the jets from AGNs and the cosmic turbulent magnetic field (Gabuzda et al. 1992; Cawthorne & Gabuzda 1996; Sol 1992; Sol & Vicente 1994, 1996; Koide et al. 1996a). To investigate the interaction between a relativistic plasma flow and a magnetic field, relativistic magnetohydrodynamics (RMHD) has often been used (Emmering & Chevalier 1987; Corbelli & Veltri 1989; Coroniti 1990; Lou 1992). However, in these theories simple models have been used, and the results are not directly applicable to relativistic jets. Relativistic hydrodynamic simulations of jets without magnetic fields have been studied by Yokosawa et al. (1982), van Putten (1993), Balsara (1994), Duncan & Hughes (1994), and Martí et al. (1995). There are few RMHD simulations that deal self-consistently with the interaction between the relativistic plasma flow and magnetic field.

In this Letter, we report on the first numerical simulation of a relativistic magnetohydrodynamic jet injected into a parallel magnetic field in a slab geometry. We have studied the morphology of relativistic jets in the cases of weak and strong magnetic fields. In the weak magnetic field jet case, the back flow is found beside the jet. On the other hand, no back flow is formed in the strongly magnetized jet. We also found that stronger reversed magnetic fields are formed in the weakly magnetized jet than in the strongly magnetized jet. These results show that the strong magnetic field collimates the jet more effectively. We also confirm that the relativistic jets propagate faster than nonrelativistic jets, even in the magnetic field.

2. RMHD EQUATIONS

The relativistic equations of conservation laws for particle number, momentum, and energy, and Maxwell equations with unit light velocity are as follows (Weinberg 1972):

$$\frac{\partial}{\partial x^{\alpha}}(nU^{\alpha}) = 0, \tag{1}$$

$$\frac{\partial}{\partial x^{\beta}}[p\eta^{\alpha\beta} + (e+p)U^{\alpha}U^{\beta} + T^{\alpha\beta}_{\rm em}] = 0, \tag{2}$$

$$\frac{\partial}{\partial x^{\alpha}}F^{\alpha\beta} = -J^{\beta}, \tag{3}$$

$$\varepsilon^{\alpha\beta\gamma\delta}\frac{\partial}{\partial x^{\beta}}F_{\gamma\delta} = 0, \tag{4}$$

where $\eta^{\alpha\beta}$ is a metric of curvature-free spacetime; $\eta^{00} = -1$, $\eta^{i} = 1$ ($i=1, 2, 3$), $\eta^{\alpha\beta} = 0$ ($\alpha \neq \beta$), and U^{α} and J^{α} are the four-velocity and four-current density, respectively. Furthermore, n, p, and e are the proper particle number density, proper pressure, and proper total energy density $e \equiv mnc^2 + p/(\Gamma - 1)$, respectively. Here Γ is the specific-heat ratio and m is the rest mass of particles. Tensor $F^{\alpha\beta}$ is defined as

$$F^{12} = B_z, \quad F^{23} = B_x, \quad F^{31} = B_y, \quad F^{01} = E_x,$$
$$F^{02} = E_y, \quad F^{03} = E_z, \quad F^{\alpha\beta} = -F^{\beta\alpha},$$

with electric field $\boldsymbol{E}$ and magnetic field $\boldsymbol{B}$. Tensor $T^{\alpha\beta}_{\rm em}$ is defined as $T^{\alpha\beta}_{\rm em} \equiv F^{\alpha}_{\gamma}F^{\beta\gamma} - \eta^{\alpha\beta}F_{\gamma\delta}F^{\gamma\delta}/4$. We cannot solve these equations in this form numerically. We change these equations to the form of explicit time evolution conservation equations. Here we include light velocity c explicitly to distinguish the relativistic effect from other effects in the simulations:

$$\frac{\partial D}{\partial t} = -\nabla \cdot (D\boldsymbol{v}), \tag{5}$$

$$\frac{\partial \boldsymbol{T}}{\partial t} = -\boldsymbol{\nabla}\cdot\left[p\boldsymbol{I} + \frac{\gamma^2}{c^2}(e+p)\boldsymbol{v}\boldsymbol{v} - \boldsymbol{B}\boldsymbol{B} - \frac{1}{c^2}\boldsymbol{E}\boldsymbol{E} + \frac{1}{2}\left(B^2 + \frac{E^2}{c^2}\right)\boldsymbol{I}\right], \quad (6)$$

$$\frac{\partial \epsilon}{\partial t} = -\boldsymbol{\nabla}\cdot\{[\gamma^2(e+p) - Dc^2]\boldsymbol{v} + \boldsymbol{E}\times\boldsymbol{B}\}, \quad (7)$$

$$\frac{\partial \boldsymbol{B}}{\partial t} = -\boldsymbol{\nabla}\times\boldsymbol{E}, \quad (8)$$

$$\frac{1}{c^2}\frac{\partial \boldsymbol{E}}{\partial t} + \boldsymbol{J} = \boldsymbol{\nabla}\times\boldsymbol{B}, \quad (9)$$

$$\frac{1}{c^2}\boldsymbol{\nabla}\cdot\boldsymbol{E} = \rho_c, \quad (10)$$

$$\boldsymbol{\nabla}\cdot\boldsymbol{B} = 0, \quad (11)$$

where $D = \gamma mn$, γ is the Lorentz factor $\gamma \equiv [1 - (v/c)^2]^{-1/2}$, and $\boldsymbol{v}$ is the velocity. Here $\boldsymbol{T}$ and ϵ are defined by

$$\boldsymbol{T} = \gamma^2\frac{e+p}{c^2}\boldsymbol{v} + \frac{1}{c^2}\boldsymbol{E}\times\boldsymbol{B}, \quad (12)$$

$$\epsilon = \gamma^2(e+p) - p - Dc^2 + \frac{1}{2}\left(B^2 + \frac{E^2}{c^2}\right). \quad (13)$$

We normalize the electric field $\boldsymbol{E}$, magnetic field $\boldsymbol{B}$, current density $\boldsymbol{J}$, and charge density ρ_c as $\boldsymbol{E} = \boldsymbol{E}^*/\sqrt{\mu}$, $\boldsymbol{B} = \boldsymbol{B}^*/\sqrt{\mu}$, $\boldsymbol{J} = \sqrt{\mu}\boldsymbol{J}^*$, and $\rho_c = \sqrt{\mu}\rho_c^*$, where $\boldsymbol{E}^*$, $\boldsymbol{B}^*$, $\boldsymbol{J}^*$, and ρ_c^* are in the MKSA unit system and μ is magnetic permeability. These equations reduce to typical Newtonian MHD equations exactly when we take the nonrelativistic limit; $c \to \infty$. Therefore we call these relativistic equations RMHD equations. The condition that the comoving electric field vanishes in a perfectly conducting plasma implies $\boldsymbol{E} = -\boldsymbol{v}\times\boldsymbol{B}$. Using the ideal RMHD assumption, we do not need to solve equation (9) explicitly. Equation (9) is used only to diagnose the current density in the ideal RMHD calculation.

Here we discuss the magnetic Reynolds number $S \equiv \tau_R/\tau_A$, where magnetic diffusion time τ_R and Alfvén transit time τ_A are defined as $\tau_R \equiv a^2/\eta$ and $\tau_A \equiv a\rho^{1/2}/B$ with characteristic electric resistivity η and scale length a, respectively. We evaluate $S = 10^{40}$ when we use the parameters: temperature $T_e = 10^5$ eV, particle number density $n_e = 10^3$ m^{-3}, magnetic field $B = 10^{-4}$ G (in extragalactic clusters), and characteristic length $a = 1$ pc (radius of a extragalactic jet). The electric resistivity is calculated by the classical Coulomb collision model (Spitzer 1962). The huge value of S means that the ideal RMHD equations are applicable to the extragalactic jets.

3. NUMERICAL METHOD

We have developed a three-dimensional RMHD numerical code that employs the *simplified total variation diminishing* (STVD) method. The STVD method was developed by Davis (1984) for violent phenomena such as shocks. This method is regarded as Lax-Wendroff's method with additional diffusion term formally. This is very useful because we need only the maximum speed of waves, and we do not need each eigenvector and its eigenvalue of the Jacobian for the time-evaluation conservation equations. We tested this method by performing a simulation of sound and magnetosonic shock waves (Koide, Nishikawa, & Mutel 1996b). We checked the energy conservation law and its propagation properties. Furthermore, we confirmed that a nonrelativistic limit with a large speed of light ($c \approx 50$) leads to the result of Newtonian calculation (nonrelativistic MHD simulation) using the calculation of Kelvin-Helmholtz instability and magnetized jet simulations.

We solve the RMHD equations numerically by the STVD method because they have conservation forms. However, we get only D, $\boldsymbol{T}$, ϵ, and $\boldsymbol{B}$ directly at each step from the different equations. For the next step, we must get $\boldsymbol{v}$ and p from D, $\boldsymbol{T}$, ϵ, and $\boldsymbol{B}$ with equations (12) and (13). For this purpose, we solve two-dimensional simultaneous algebraic equations with unknown variables $x \equiv \gamma - 1$ and $y \equiv \gamma(\boldsymbol{v}\cdot\boldsymbol{B})/c^2$,

$$x(x+2)\left[\Gamma a x^2 + (2\Gamma a - b)x + \Gamma a - b + d + \frac{\Gamma}{2}y^2\right]^2 = (\Gamma x^2 + 2\Gamma x + 1)^2[\tau^2(x+1)^2 + 2\sigma y + 2\sigma x y + \beta^2 y^2], \quad (14)$$

$$\left[\Gamma(a - \beta^2)x^2 + (2\Gamma a - 2\Gamma\beta^2 - b)x + \Gamma a - b + d - \beta^2 + \frac{\Gamma}{2}y^2\right]y = \sigma(x+1)(\Gamma x^2 + 2\Gamma x + 1), \quad (15)$$

where $a = D + \epsilon/c^2$, $b = (\Gamma - 1)D$, $d = (1 - \Gamma/2)B^2/c^2$, $\tau = T/c$, $\beta = B/c$, and $\sigma = \boldsymbol{B}\cdot\boldsymbol{T}/c^2$. It is noted that in the absence of the magnetic field, equation (14) becomes the equation in the relativistic hydrodynamic case as derived by Duncan & Hughes (1994), and equation (15) becomes a trivial equation. We cannot solve these algebraic equations analytically. The equation is solved at each cell using the two-dimensional Newton-Raphson iteration method. In our code, we use double precision in the subroutine of this iteration. We can easily calculate p and $\boldsymbol{v}$ using x, y, D, $\boldsymbol{T}$, ϵ, and $\boldsymbol{B}$.

4. NUMERICAL RESULTS

We present a two-dimensional simulation of relativistic jets injected into parallel magnetic fields. We perform calculations for two cases where the magnetic fields are so strong and weak that the magnetic energy density is comparable to, and 1/16 of, the rest mass energy density, respectively. Initially, the rest mass density, pressure, and magnetic field are uniform. The initial magnetic field is directed in the x-direction.

The jet is injected from the orifice at the left boundary of the calculation box, $x = 0$, $-1 \le y \le 1$. The left surface $x = 0$ is bounded by fixed boundary condition. Boundary conditions of $x = 20$, $y = \pm 10$ surfaces are radiative boundary conditions. We use periodic boundary conditions along the z-direction for the slab geometry. The proper Mach number of the injection velocity for the both cases [$M_s = V_{jet}/v_s$, $v_s \equiv (\Gamma p/mn)^{1/2}$] is 4, which corresponds to the Lorentz factor of 4.56. The ratio of jet rest mass density to ambient density η is 0.3. The simulation is continued until $t = 10\tau_s$ where τ_s is the transit time of sound wave to unit distance. The simulation was performed at an intermediate resolution of $81 \times 81 \times 3$ grid points. The computations were performed on a Fujitsu VPX210/10S mini–super computer with 16 M byte internal memory and required 20 minutes of CPU time for 200 time steps.

Figures 1 and 2 show the velocity (panels a), magnetic field (panels b), rest mass density (panels c), and pressure (panels d) of the two cases at the same time $t = 6\tau_s$. The Mach disks are formed at $x \sim 15$ in both cases (Figs. 1c–2c). The locations of the Mach disks are almost the same in both cases

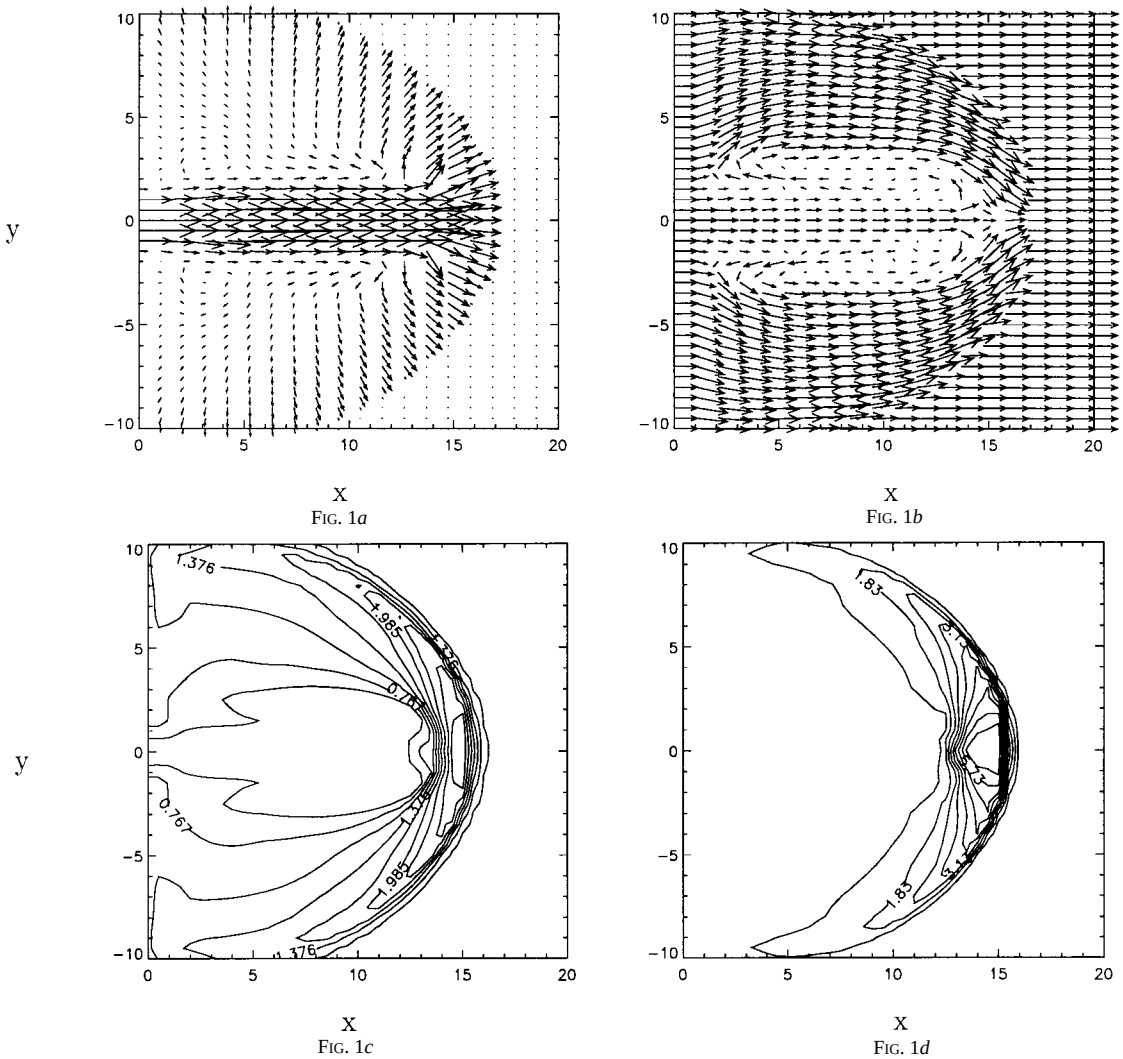

FIG. 1*a* FIG. 1*b*

FIG. 1*c* FIG. 1*d*

FIG. 1.—A snapshot of a weakly magnetized jet simulation at $t = 6\tau_s$: (*a*) the velocity, (*b*) magnetic field, (*c*) density, and (*d*) pressure. The jet is injected from the left boundary with proper Mach number (M_s) 4, which corresponds to a Lorentz factor of 4.56. We can see back flow beside the jet. The jet material spreads transversely along the back flow. A strongly bent magnetic field is found near the jet.

and the propagation velocities of the relativistic jets are almost the same: $v_h = 2.67\ v_s$. The propagation velocities are larger than that of the Newtonian jet $v_h = \sqrt{\eta}(1 + \sqrt{\eta})^{-1} v_{jet} = 1.42\ v_s$ because the Lorentz contraction increases the jet effective mass density. The transversal propagation of the bow shock of the strong magnetic field case is faster than that of weak magnetic field case (Figs. 1*c*, 1*d*, 2*c*, 2*d*). This is because the magnetosonic wave of the strong magnetic field case is faster than that of the weak magnetic field case.

Figure 1*a* shows that the back flow is formed beside the jet in the weak magnetic field case. The jet material spreads transversely along the back flow. The back flow forms a cocoon similar to that of a relativistic hydrodynamic jet without a magnetic field as reported by van Putten (1993). The whole flow of this case is the same as of a case with no magnetic field case (which is not presented in this Letter), which means that the weak magnetic field has no influence on the jet propagation. On the other hand, there is no back flow in the strongly magnetized jet, as shown in Figure 2*a*. This shows that the strong magnetic field confines the jet. As shown in Figures 1*b* and 2*b*, the magnetic field is reversed beside the jet for both cases. The area of the reversed magnetic field of the strong magnetic field case is smaller than that of the weak magnetic field case. This is because the Alfvén velocity of the strong magnetic field case is almost the same as the speed of light, and the hair-pin area of the magnetic field follows the jet head quickly while it is not in the weak magnetic field case. The density at the Mach disk of the weak magnetic field case is larger than that of the strong magnetic field case (Figs. 1*c*–2*c*). The high-pressure region of the weak magnetic field case is localized around the jet head (Fig. 1*d*). This morphology of Mach disk of weakly magnetized relativistic jet is similar to that of the hydrodynamic relativistic jet, as shown by van Putten (1993). On the other hand, it spreads along the jet in the strong magnetic field case (Fig. 2*d*). This also shows the slight influence of the weak magnetic field on the jet and the confinement of the jet by the strong magnetic field.

The results show that both the strong parallel magnetic field and the relativistic effect collimate the jet, and consequently the jet propagates further without slowdown. This may explain the observational properties of jets from most quasars, which are straighter, smoother, and faster than the ones from BL Lacertae objects. On the other hand, for bending extragalactic jets, such as the jets from 3C 279, 3C 454.3 (Cawthorne & Gabuzda 1996), and BL Lacertae objects (Mutel 1989), a jet propagation into a oblique magnetic field is important as one of their bending mechanisms (Sol 1992; Sol & Vicente 1994, 1996), as was found by the nonrelativistic MHD simulation

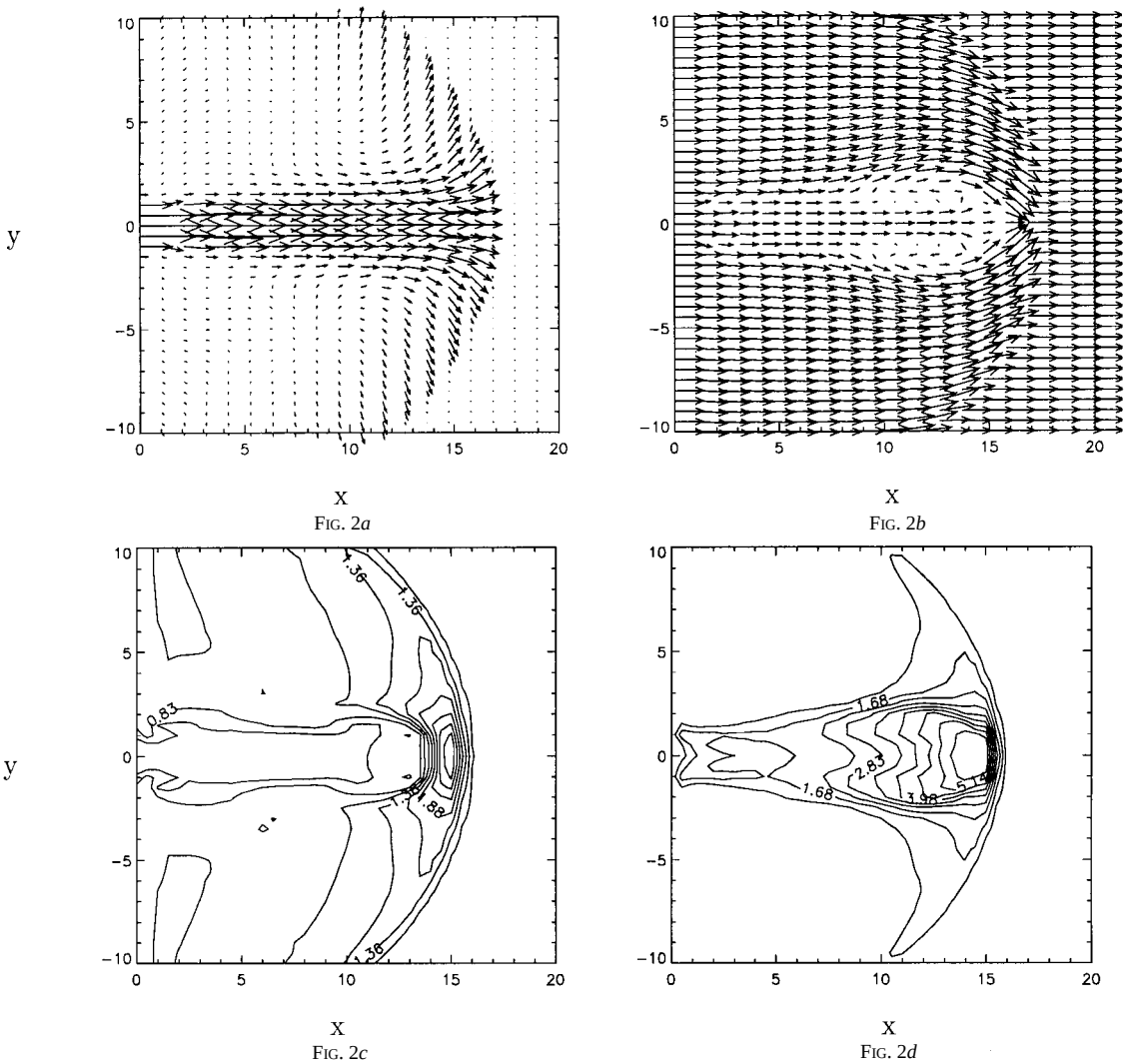

FIG. 2.—A snapshot of a strongly magnetized jet simulation at $t = 6\tau_s$: (*a*) the velocity, (*b*) magnetic field, (*c*) density, and (*d*) pressure. The jet is injected from the left boundary with proper Mach number (M_s) 4, which corresponds to a Lorentz factor of 4.56. We found no back flow in this case. The jet material is confined by the strong magnetic field. We note that the scales of the vectors in Figs. 1*a*–1*b* and Figs. 2*a*–2*b* are different.

(Koide et al. 1996a). In this case, the three-dimensional effect also becomes important. A long-term simulation with a radiation effect is needed to compare further the numerical results to the observations of extragalactic jets (Gómez et al. 1995). We intend to include these effects in our future work.

We thank Jun-Ichi Sakai for his encouragement. We also thank Philip Hardee and Alex Rosen for their kindness and helpful discussions at Alabama Workshop on Energy Transport in Radio Galaxies and Quasars. One of us (S. K.) thanks Mika Inda-Koide for her important comments. This work is supported by the US-Japan cooperative science program JSPS and NSF (INT-9117650). K.-I. N. is supported by the National Science Foundation under Grant Nos. ATM-9119814 and ATM-9121116.

REFERENCES

Balsara, D. S. 1994, J. Comput. Phys., 114, 284
Burns, J. O., Norman, M. L., & Clarke, D. A. 1991, Science, 253, 522
Cawthorne, T. V. 1991, in Beams and Jets in Astrophysics, ed. P. A. Hughes (Cambridge: Cambridge Univ. Press), 187
Cawthorne, T. V., & Gabuzda, D. C. 1996, MNRAS, in press
Corbelli, E., & Veltri, P. 1989, ApJ, 340, 679
Coroniti, F. V. 1990, ApJ, 349, 538
Davis, S. F. 1984, NASA Contractor Rep. 172373, ICASE Rep., No. 84-20
Duncan, G. C., & Hughes, P. A. 1994, ApJ, 436, L119
Emmering, R. T., & Chevalier, R. A. 1987, ApJ, 321, 334
Gabuzda, D. C., Cawthorne, T. V., Roberts, D. H., & Wardle, J. F. C. 1992, ApJ, 388, 40
Gabuzda, D. C., Wardle, J. F. C., & Roberts, D. H. 1989, ApJ, 336, L59
Gómez, J. L., Martí, J. M., Marscher, A. P., Ibáñez, J. M., & Marcaide, J. M. 1995, ApJ, 449, L19
Hardee, P. E. 1987, ApJ, 318, 78
Hardee, P. E., & Clarke, D. A. 1995, ApJ, 451, L25
Koide, S., Nishikawa, K.-I., & Mutel, R. L. 1996b, in preparation
Koide, S., Sakai, J.-I., Nishikawa, K.-I., & Mutel, R. L. 1996a, ApJ, 464, in press
Lou, Y.-Q. 1992, ApJ, 397, L67
Martí, J. M., Müller, E., Font, J. A., & Ibáñez, J. M. 1995, ApJ, 448, L105
Mutel, R. L. 1989, in Proc. Parsec-Scale Radio Jet Workshop (Socorro, NM), ed. J. A. Zensus & K. I. Kellermann (Green Bank: National Radio Astronomy Obs.) 191
Mutel, R. L., Phillips, R. B., Su, B., & Bucciferro, R. R. 1990, ApJ, 352, 81
Sol, H. 1992, in Extragalactic Radio Sources from Beams to Jets, ed. J. Roland, L. Sol, & G. Pelletier (Cambridge: Cambridge Univ. Press), 264
Sol, H., & Vicente, L. 1994, in IAU Symp. 159, Multiwavelength Continuum Emission of AGN, ed. T. J.-L. Courvoisier & A. Blecka (Dordrecht: Kluwer), 473
———. 1996, A & A, submitted
Spitzer, L. J. 1962, Physics of Fully Ionized Gases (New York: Interscience)
van Putten, M. H. P. 1993, ApJ, 408, L21
Weinberg, S. 1972, Gravitation and Cosmology (New York: Wiley)
Yokosawa, M., Ikeuchi, S., & Sakashita, S. 1982, PASJ, 34, 461